Scientific Research Publishing

Journal of Materials Science and Chemical Engineering, 2023, 11, 73-90
https://www.scirp.org/journal/msce
ISSN Online: 2327-6053
ISSN Print: 2327-6045

# Creation of a Novel Piezoelectric Nanogenerator for Sensory Receptor Damage Treatments

**Annika Joshi**

Johns Creek High School, Johns Creek, GA, USA
Email: annikajoshi123@gmail.com

**How to cite this paper:** Joshi, A. (2023) Creation of a Novel Piezoelectric Nanogenerator for Sensory Receptor Damage Treatments. *Journal of Materials Science and Chemical Engineering*, **11**, 73-90.
https://doi.org/10.4236/msce.2023.117005

**Received:** June 4, 2023
**Accepted:** July 28, 2023
**Published:** July 31, 2023



## Abstract

Every year, millions of people incur damage to sensory receptors that interact with the external environment. Two areas of concern are hearing loss (affecting around 430 million) and burns (affecting 11 million annually). Current treatments for burns involve skin grafts, which are expensive and prone to rejection by the body. Current treatments for hearing loss involve implants and hearing aids, which have limited sensitivity, need batteries and charging, are expensive, and are prone to infection. Thus, there is a need for a self-powered, flexible, biocompatible, antibacterial, and inexpensive solution that can respond to stimuli at a rate comparable to tissue. Piezoelectric materials convert mechanical energy into electricity, thus replicating touch and hearing by simulating nerve signals. In this study, piezoelectric membranes with varying ratios of polyvinylidene fluoride (PVDF) and zinc oxide (ZnO) were fabricated using electrospinning. These membranes were characterized with scanning electron microscopy (SEM), X-ray diffraction (XRD), Fourier transform infrared spectroscopy (FTIR), stress-strain analysis, and piezoresponse testing. Results showed that increasing the amount of PVDF made the membrane more flexible but reduced its piezoelectric potential (decrease in PVDF $\beta$-phase). Increasing the amount of ZnO significantly increased piezoelectric potential (increase in PVDF $\beta$-phase) but degraded the flexibility and usability of the membrane. Therefore, a 1:1 w/w ratio of PVDF to ZnO is the optimum ratio for balancing both piezoelectric potential and flexibility. These results support the hypothesis that composites of PVDF and ZnO can help realize self-powered hearing rehab devices and wearable electronic skin.

## Keywords

Wearable Electronic Skin, Hearing Rehab, Piezoelectric Membranes, Flexible Membranes, Nanogenerator, Self-Powered Nanogenerator

# 1. Introduction

## 1.1. Current Problems

According to the World Health Organization (WHO), burns affect around 11 million people annually. Burns impact low-income countries up to 7 times more than high-income nations [1]. This general disparity holds true in the U.S. as well in low-income districts, 23.4 people per 100,000 are hospitalized for burns, as compared to 14.1 per 100,000 in middle- and high-income areas [1]. About 1/3 of treatments for burn-related inpatient stays in the U.S. include skin grafts [2]. Despite some advancements, this treatment is still riddled with issues. Engineered tissue and immunosuppressive treatments have reduced the risk of early graft rejection, but first-set rejection, after 1 - 2 weeks, remains common [3]. Additionally, bacterial infections occur frequently [4].

Another medical problem worldwide is hearing loss. By 2050, around 700 million people worldwide will have hearing loss requiring rehab, and around 2.5 billion people will have some hearing loss [5] according to the WHO. 30 million of these people are in the United States [5]. Hearing loss rehab includes hearing aids, cochlear implants, and middle ear implants. However, implants have low sensitivity [6], require batteries [6], and are expensive [7].

## 1.2. Potential Solution

There is a need for engineered solutions that can help alleviate these problems and improve the quality of life for millions of people with these medical conditions. Any solution would need to be able to mimic the characteristics of human skin and tissue, such as detecting a variety of tactile stimuli (*i.e.* touch, pressing, slippage, bending, vibrations, etc.), responding to stimuli at a rate comparable to human tissue [8], and passing on the stimuli to the nervous system. Biological tissue is contoured, with varying textures, and electronic skins must be thin and flexible to achieve maximum contact ("conformal contact") with the human body part in question [9]. The engineered tissue would need to be antibacterial, as it will be in contact with damaged skin in the case of burns or the inner mucosa of the ear in the case of hearing loss [10].

The piezoelectric effect refers to the natural conversion of mechanical energy to electricity within a material. It can also, conversely, refer to the deformation in a material when an electric field is applied [11]. This effect can be used to connect a piezoelectric membrane to underlying neural tissue, as it can transfer charge to the site-specific nerve non-invasively in response to mechanical forces [12].

This led to the following goal: To develop a self-powered, flexible, biocompatible, antibacterial, and piezoelectric membrane that can be used to mimic human sensory receptor tissue.

## 1.3. Design Choices

A literature survey was performed to determine which materials to use. Mate-

rials were chosen from a list of 20 potential candidates based on their physical properties, their piezoelectric or self-powered potential, biocompatibility, antibacterial characteristics, flexibility to conform to the human body, and novelty. Polyvinylidene fluoride (PVDF) is a semi-crystalline polymer that can exist in four different phases known as: $\alpha$, $\beta$, $\gamma$, and $\delta$ [13]. The most stable and commonly found one is the $\alpha$-phase, which is amorphous and does not possess piezoelectric properties. The $\beta$-phase exhibits strong piezoelectric properties and is the most significant one for this study [13]. Usually, PVDF will be majority $\alpha$-phase, with small amounts of $\beta$- and $\gamma$-phases [13]. Any membrane developed would need to maximize the piezoelectric potential of PVDF by increasing the $\beta$-phase. PVDF is also biocompatible [14], flexible [14], and non-hazardous [15]. We also selected zinc oxide (ZnO) as the second material in the study as it is biocompatible [16], piezoelectric [17], and antibacterial [18]. However, ZnO is not very flexible and tends to be brittle [19]. Bulk ZnO also has a low piezoelectric coefficient while ZnO nanostructures show increased piezoelectric activity [20]. Thus, we decided to combine PVDF and ZnO nanoparticles to create a composite with higher piezoelectric potential and greater antibacterial action than PVDF by itself, and a higher flexibility than ZnO by itself.

Composite membranes are typically prepared by dissolving materials in a solvent to create a homogeneous solution and then removing the solvent in a controlled manner [21]. A solvent was needed to make a homogeneous solution of PVDF and ZnO. Dimethylformamide (DMF) was the solvent used most frequently in the established studies reviewed. However, it is a strong toxin that can cause severe vomiting, dizziness, liver injury, and more [22]. Thus, the decision was made to use dimethyl sulfoxide (DMSO) instead, as it is also a strong solvent for PVDF [23] and is in the safest category for solvents (class 3, lowest toxicity) [24]. Additionally, acetone was used in combination with DMSO, as it is a solvent for PVDF and can improve the viscosity of the overall solution [23].

Electrospinning is a technique in which a syringe pump sprays a solution through an electric field, thus causing the solution fibers to be pulled onto a metal collector [25]. Electrospinning has tremendous potential in the biomedical field, as it can create membranes that can be tailored to match biological tissues in their properties [25]. These membranes can conform well to large surface areas of the body [26].

### 1.4. Research Question and Hypothesis

The research question is what is the optimum ratio of PVDF to ZnO for improving sensory reception using piezoelectricity? The hypothesis of this study is that changing the amount of ZnO will change the piezoelectric potential of PVDF.

### 1.5. Variables

The independent variable in this study was the ratio of PVDF to ZnO. The dependent variables in this study include viscosity, homogeneity, piezoelectric po-

tential ($\beta$-phase percentage and crystallinity), and flexibility. The control variables are materials, solvents, equipment, equipment settings, and temperature. To the best of our knowledge, there has been no prior study on testing ratios of PVDF to ZnO for this purpose.

## 2. Materials and Methods

### 2.1. Materials

Ethanol (Sigma-Aldrich®), Zinc acetate dihydrate 98% extra pure (Thermo Scientific™), Sodium Hydroxide (Sigma-Aldrich®), Poly(vinylidene fluoride) (Sigma-Aldrich®), Dimethyl sulfoxide (Fisher Chemical®), Acetone (Sigma- Aldrich®), Distilled water.

### 2.2. Preparation of ZnO Nanoparticles by Sol-Gel Method

ZnO crystals were precipitated using a sol-gel process described in [27]. 2 g of zinc acetate dihydrate was dissolved in 15 mL of distilled water. 8 g of sodium hydroxide was dissolved in 10 mL of distilled water. Both solutions were stirred for 5 minutes together. Then, 100 mL ethanol was added to the combined solution drop by drop until ZnO crystals were precipitated. These white precipitates were filtered and dried. This process was repeated to obtain sufficient ZnO.

### 2.3. Preparation of PVDF and ZnO Membranes

Three different solutions of varying ratios of PVDF and ZnO were prepared:

M1: 12% PVDF (2.4 g), 22% ZnO (4.4 g), 66% DMSO/Acetone (3.3 g DMSO + 9.9 g acetone).

M2: 17% PVDF (3.4 g), 17% ZnO (3.4 g), 66% DMSO/Acetone (3.3 g DMSO + 9.9 g acetone).

M3: 22% PVDF (4.4 g), 12% ZnO (2.4 g), 66% DMSO/Acetone (3.3 g DMSO + 9.9 g acetone).

3.3 g of DMSO and 9.9 g of acetone were mixed to make a 13.2 g solvent mixture. The required amount of PVDF was added to this mixture and magnetically stirred using a DLAB MS-H280-Pro for 2 hours to make a homogeneous solution. After this, the required amount of ZnO was added to the solution, and the entire solution was stirred for 1 hour. Solutions were sonicated using a Sonics Vibra-cell VCX 750 sonicator. Membranes were then electrospun using a Spellman H.V. and a Razel R-100E syringe pump on an aluminum foil collector. Parameters decided upon involved using an applied voltage of 18 kV, tip to collector distance of 15 cm, flow rate 0.8 mL/h, and collector speed of 500 rpm based upon a review of existing literature in the field [28], as well as feedback from the lab technician. Characterization tests were carried out on these electrospun membranes.

### 2.4. Characterization of Membranes

Samples of 1 inch by 1 inch were used for SEM Imaging. 10 to 20 SEM images were

obtained per sample using a Phenom ProX G6, Netherlands, at a voltage of 15 kV.

Samples of 2 inches by 2 inches were used for XRD analysis on a Bruker D2 Phaser, using 30 kV and 10 mA. XRD results were pulled into Excel and a Y-offset of 20 K and 125 K were added to M2 and M3 for to create separation in the combined stacked chart for analysis.

Samples of 2 inches by 2 inches were used for FTIR analysis. FTIR analysis was done using a ThermoFisher Scientific Nicolet 6700. 128 scans were performed at various locations within each sample and averaged to get the final spectrums. FTIR results were pulled into Excel and a Y-offset of 1, 2 and 3 were added to M1, M2 and M3 to create separation in the combined stacked chart for analysis.

Tensile stress testing was performed on samples of 2 inches by 0.5 inch using a TestResources 1000 lb actuator with a SM-250-294 force transducer.

All characterizations were done at room temperature and the same machine/settings were used for all samples.

## 3. Results

### 3.1. Visual Analysis

The solution for M1 was highly viscous, and difficult to use. Membranes prepared were flaky (Figure 1) and tended to stick to the aluminum foil collector (Figure 2). Membranes prepared with these solutions were smooth and did not stick to the aluminum foil collector (Figure 3, Figure 4).

### 3.2. SEM Analysis

SEM images of all three membranes were taken and showed surface morphology (Figures 5-8).

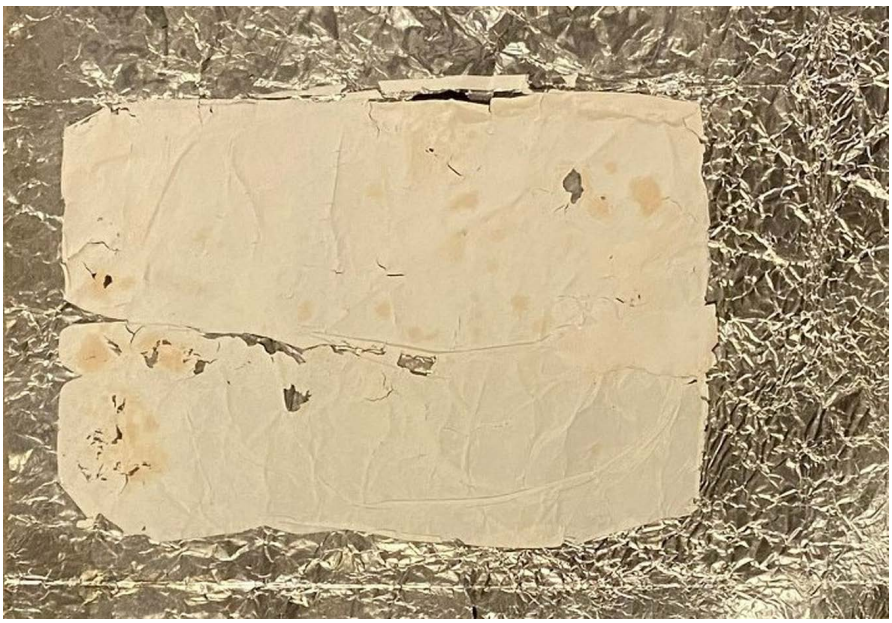

Figure 1. M1 (membrane prepared with 12% PVDF and 22% ZnO w/w). Note flakes and tears.

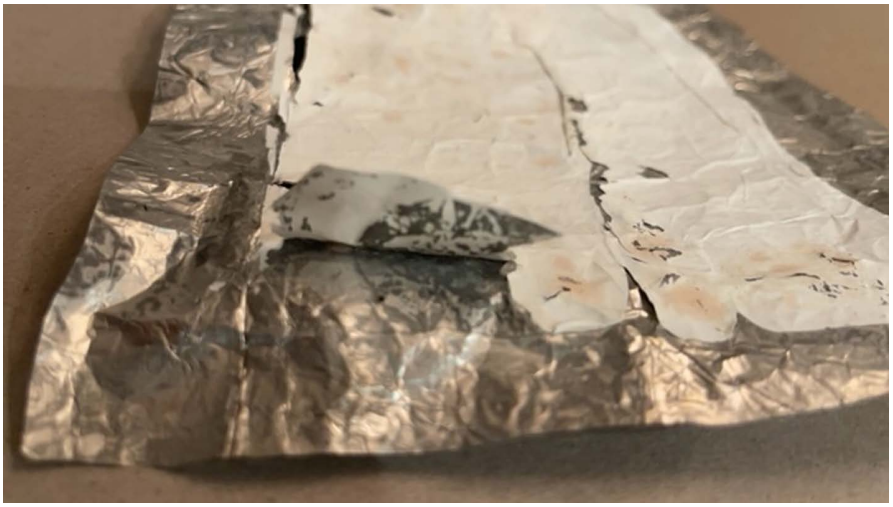

Figure 2. M1 (membrane prepared with 12% PVDF and 22% ZnO w/w). Note how membrane sticks to aluminum foil.

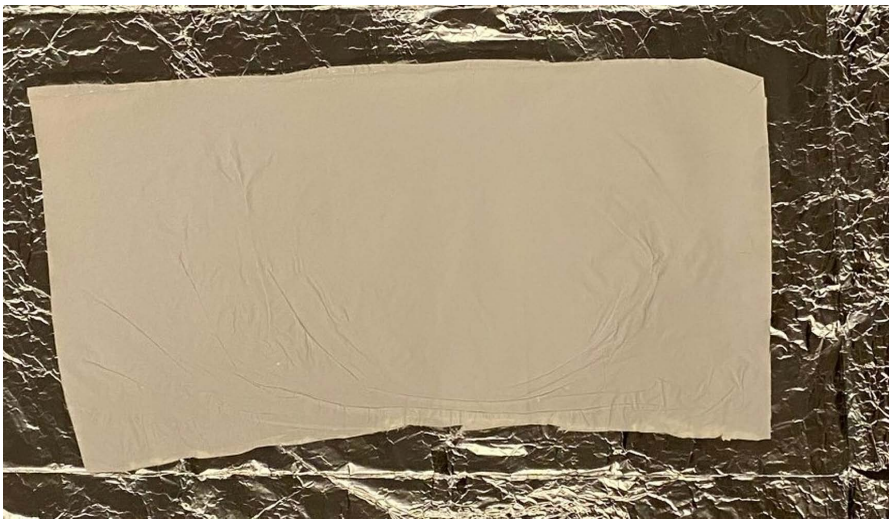

Figure 3. Electrospun membrane M2 (membrane with 17% PVDF and 17% ZnO w/w).

Figure 4. Electrospun membrane M3 (membrane with 22% PVDF and 12% ZnO w/w).

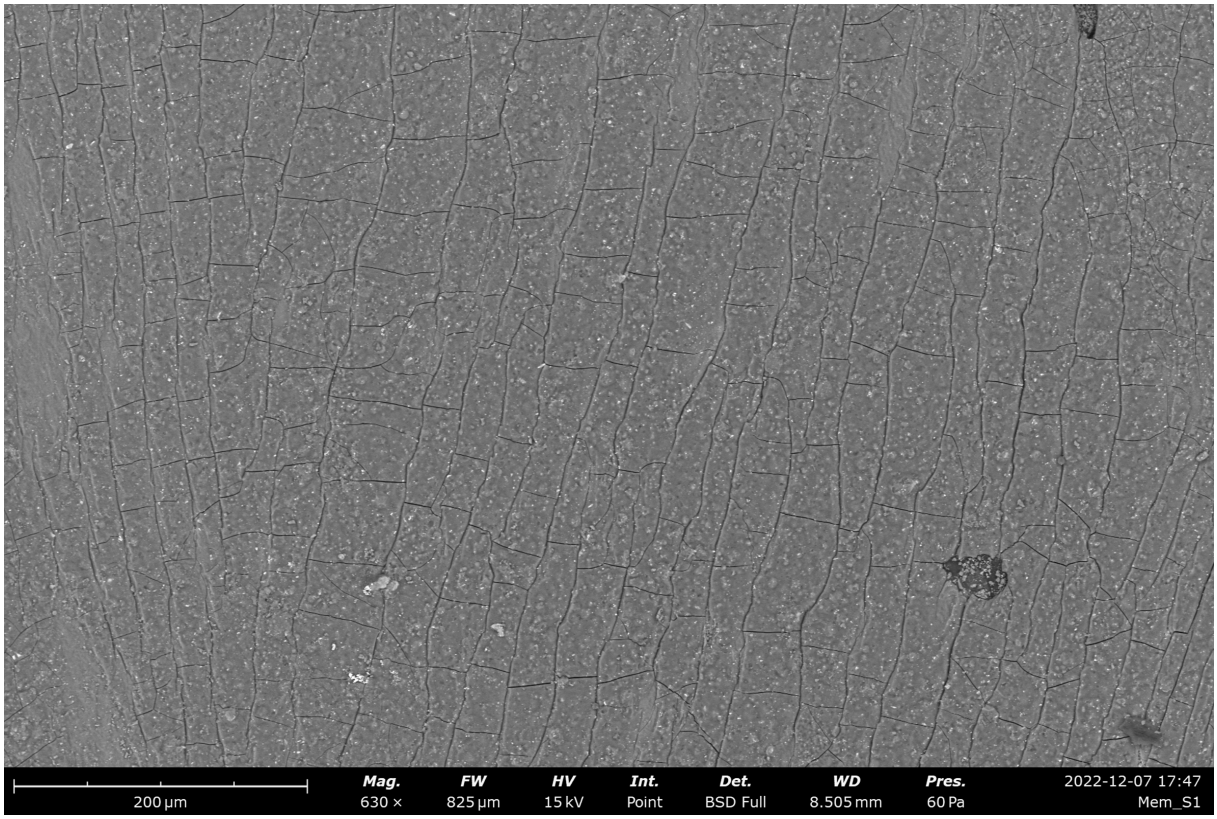


Figure 5. SEM image of M1 (membrane with 12% PVDF and 22% ZnO w/w). Note visible cracks on surface.

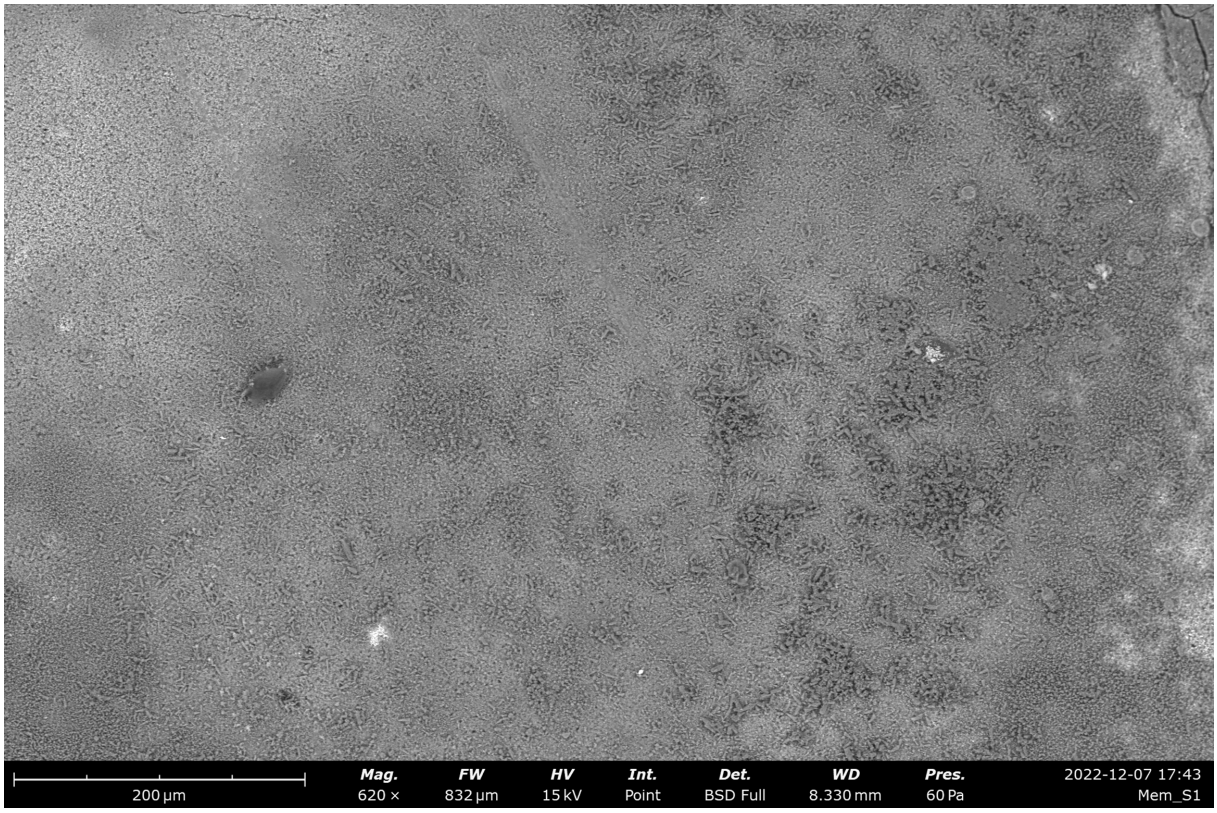


Figure 6. SEM image of M1 (membrane with 12% PVDF and 22% ZnO w/w). Note visible clumps.

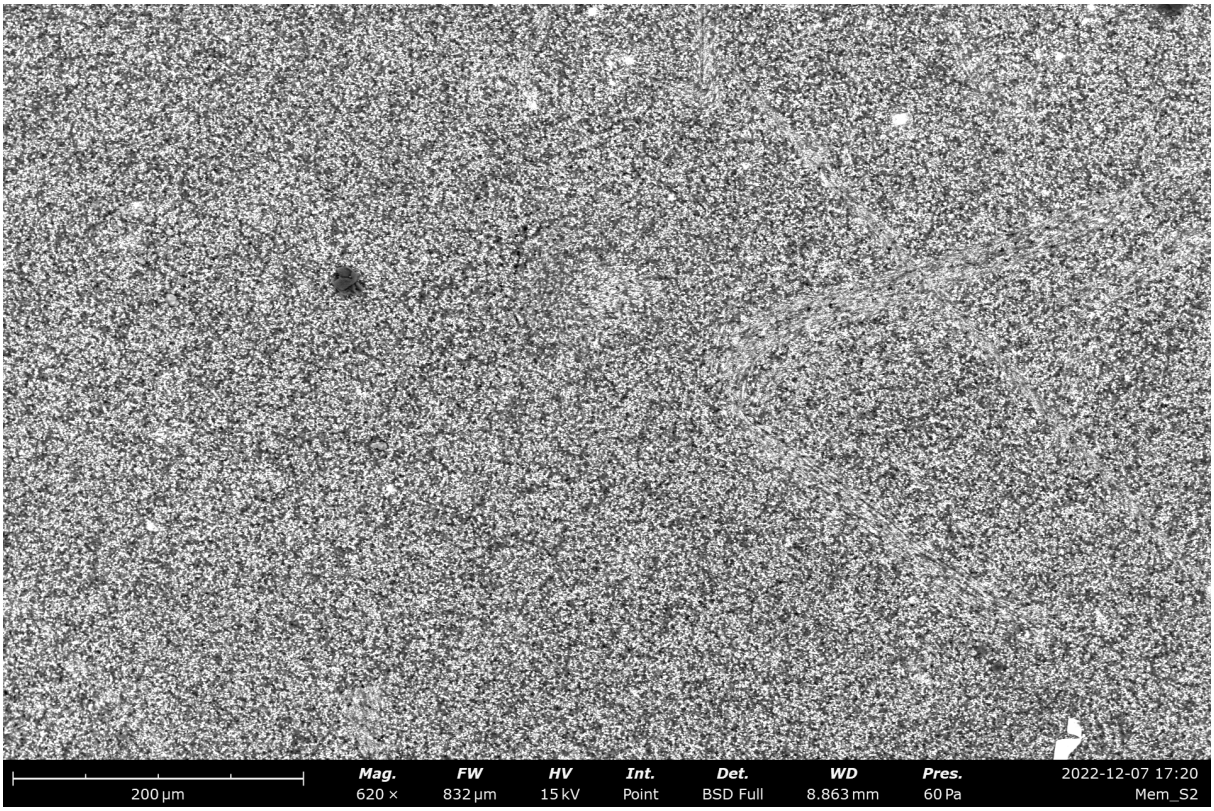


**Figure 7.** SEM image of M2 (membrane with 17% PVDF and 17% ZnO w/w). No surface cracks, and homogenous.

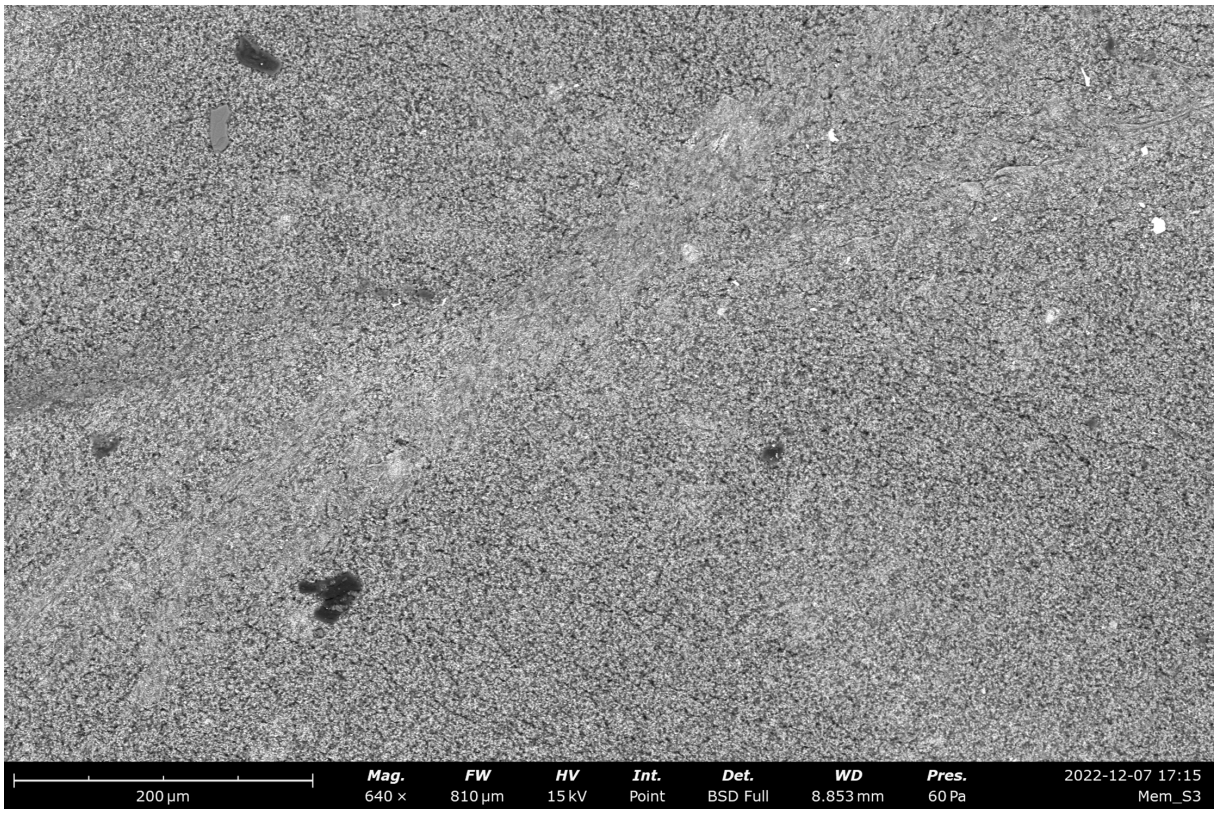


**Figure 8.** SEM image of M3 (membrane with 22% PVDF and 12% ZnO w/w). No surface cracks, and homogenous.

### 3.3. XRD Analysis

The stacked XRD diffraction pattern for all three membranes is shown in Figure 9. The diffraction pattern for M2 and M3 was Y-offset for clarity. The diffraction peak at $2\theta = 20.54^{\circ}$ is characteristic of the $\beta$-phase [29] [30]. The diffraction peaks at $2\theta = 31.9^{\circ}$, 34.64, 36.5, 47.7, 56.7 are characteristic of ZnO [31].

### 3.4. Open Specy Analysis

The FTIR absorption spectra for all three membranes were imported into Open Specy, an open access web-based spectroscopy analysis tool [32]. FTIR absorption spectra for each membrane were plotted for comparative analysis against the FTIR absorption spectra for PVDF by itself (Figures 10-12).

### 3.5. FTIR Analysis

FTIR analysis was performed to study the percentage of piezoelectric $\beta$-phase in the membranes. FTIR absorption data was imported into Excel for analysis and charting. The absorption data for M2 and M3 was Y-offset for clarity. Figure 13 shows the spectra of the three membranes between 600 $cm^{-1}$ and 1500 $cm^{-1}$ as this is the region of interest for analysis.

### 3.6. Tensile Testing Analysis

Tensile testing was performed on M2 and M3, as M1 was determined brittle. Data was imported into Excel for analysis. Load-displacement graphs are shown in Figure 14.

## 4. Discussion and Conclusions

### 4.1. Visual Findings

The solution for M1 was difficult to spread due to its viscosity. As a result, the

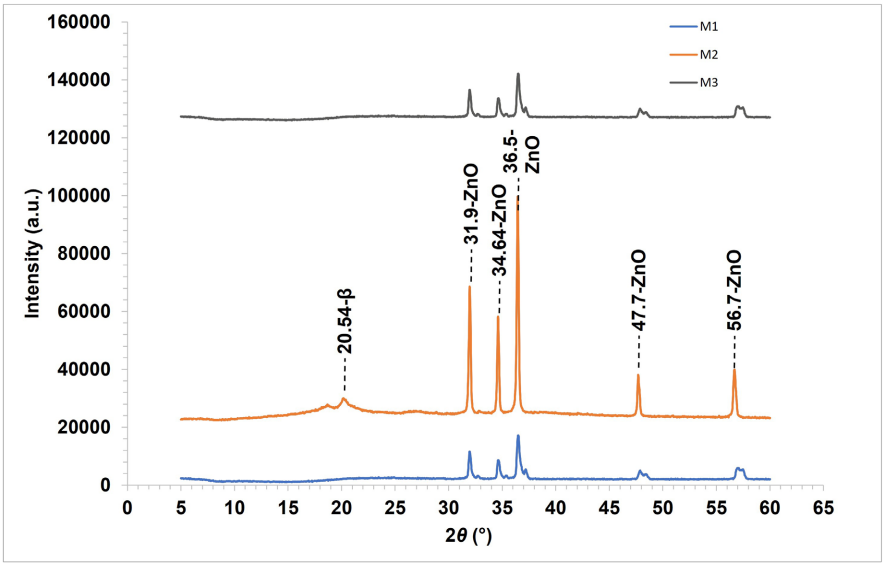


Figure 9. XRD stacked chart for all three membranes.

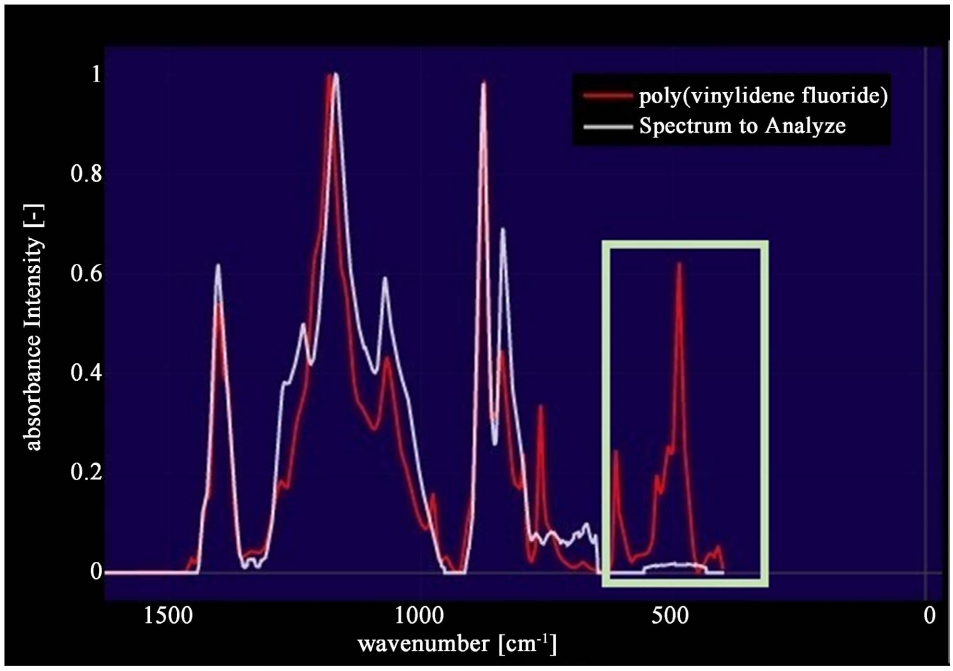


**Figure 10.** Open Specy comparison of FTIR absorption spectra in the range of wavenumbers 0 - 1500 for M1 (membrane with 12% PVDF and 22% ZnO w/w) to PVDF. Rectangular boxed area shows section from 0 - 600 where *α*-phase peaks were eliminated.

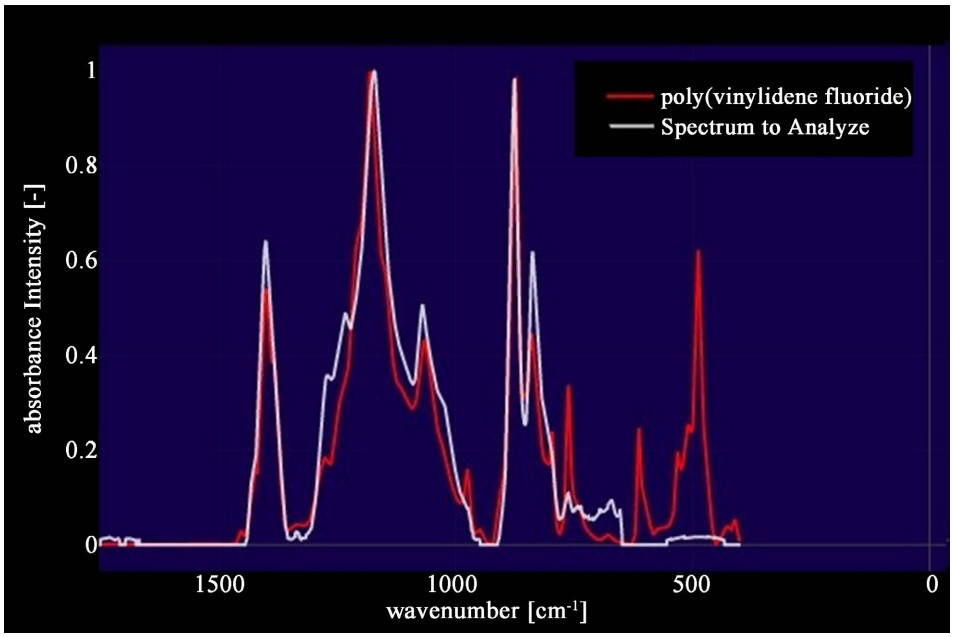


**Figure 11.** Open Specy comparison of FTIR absorption spectra in the range of wavenumbers 0 - 1500 for M2 (membrane with 17% PVDF and 17% ZnO w/w) to PVDF.

membrane tended to dry out quickly, broke into flakes (Figure 1), and could not be separated from the aluminum foil collector (Figure 2). Membranes prepared with these solutions were smooth and did not stick to the aluminum foil collector (Figure 3, Figure 4). This indicates that the ratio in M1 is not suitable for use while M2 and M3 are usable.

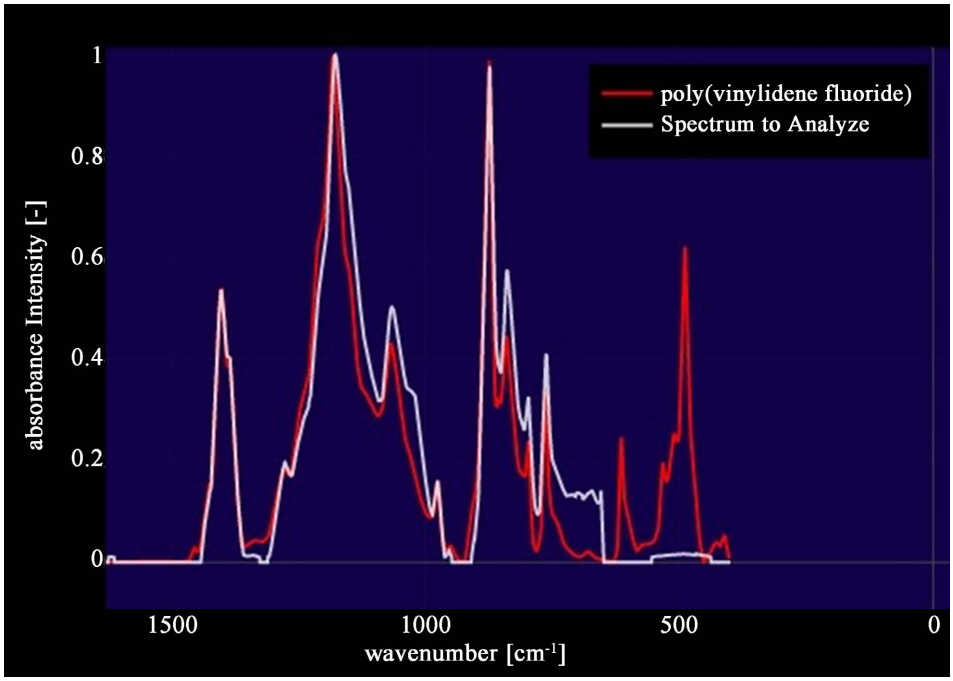


Figure 12. Open Specy comparison of FTIR absorption spectra in the range of wavenumbers 0 - 1500 for M3 (membrane with 22% PVDF and 12% ZnO w/w) to PVDF.

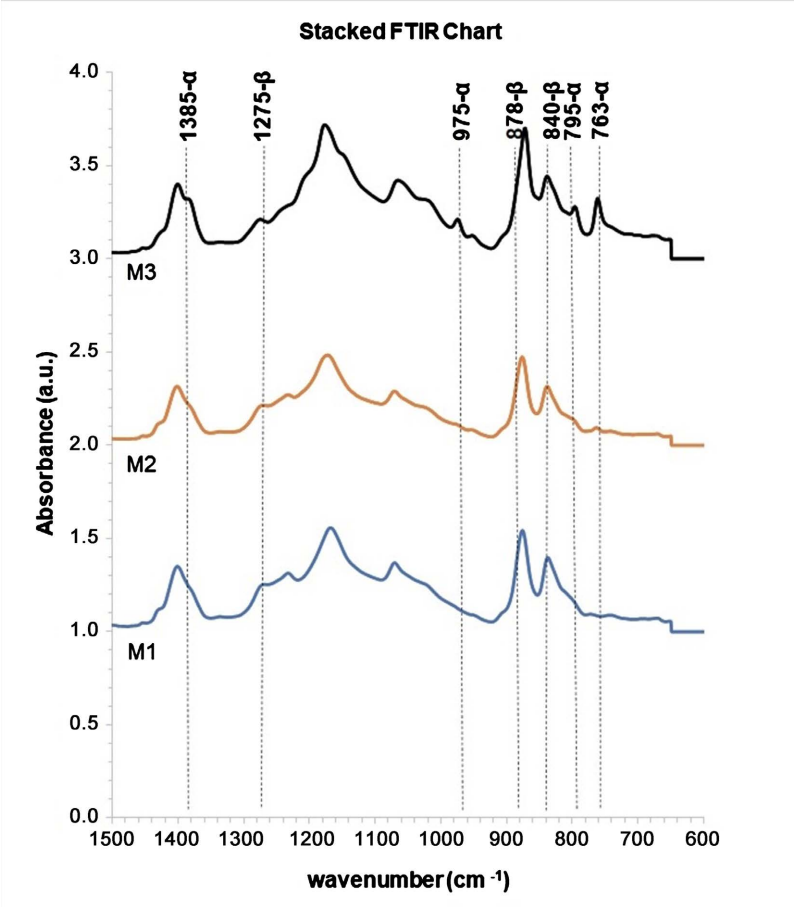


Figure 13. FTIR stacked chart.

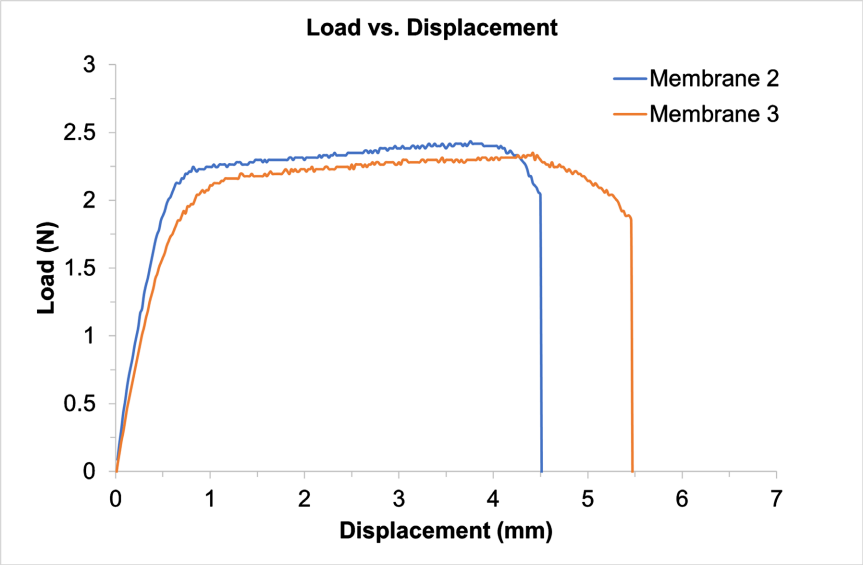


Figure 14. Load-displacement graph.

### 4.2. SEM Findings

Surface morphology of M1 is rough, with small cracks throughout the surface (Figure 5). There are large clumps of ZnO and PVDF on the surface of M1, which appear as micrometer-sized particles (Figure 6). Surfaces for M2 and M3 appear uniform, suggesting a better dispersion of ZnO and PVDF (Figure 7, Figure 8). These results indicate, again, that M2 and M3 are homogeneous and more usable than M1.

### 4.3. XRD Findings

The XRD stacked chart (Figure 9) shows a strong diffraction peak for M2 at $2\theta$ = 20.54˚. This indicates that $\beta$-phase in M2 is highly crystalline which in turn implies a high degree of piezoelectric potential. Conversely, neither M1 nor M3 show this strong diffraction peak at $2\theta$ = 20.54˚ which indicates that they have a lower degree of crystallinity than M2. Diffraction peaks at $2\theta$ = 31.9˚, 34.64˚, 36.5˚, 47.7˚, 56.7˚ are visible on all three membranes, which means that ZnO retained its crystallinity and the addition of PVDF did not alter it in anyway.

### 4.4. Open Specy Findings

FTIR data for M1, M2, and M3 were uploaded to the Open Specy tool and compared individually to the known spectrum for PVDF. There were no added peaks for the composite membranes (Figures 10-12), which indicates that the reaction was physical, not chemical, and no new compounds were created in the process. $\beta$-phase peak intensity in M1, M2, and M3 were higher than with only PVDF, suggesting that the addition of ZnO increased crystallization (Figures 10-12) in all instances. Moreover, non-piezoelectric $\alpha$-phase peaks in range 0 - 600 were eliminated (Figures 10-12, rectangular boxed area) which implies that the addition of ZnO resulted in an overall reduction in non-piezoelectric $\alpha$-phase in all

three ratios.

### 4.5. FTIR Findings

FTIR analysis was performed to study the percentage of PVDF piezoelectric $\beta$-phase in the membranes. Phases of PVDF can be discerned by using the methodology outlined in [28]. Peaks exclusive to the piezoelectric $\beta$-phase were detected in all three membranes at wavenumber = 840, 878 and 1275 (**Figure 13**). Peaks at wavenumber = 763 which are exclusive to the non-piezoelectric $\alpha$-phase, were also detected in all three membranes (**Figure 13**). Thus, some quantity of $\alpha$-phase is present in all three membranes. However, $\alpha$-phase peaks were also detected at 796, 975, and 1385 in M3 (**Figure 13**). Thus, there is more non-piezoelectric $\alpha$-phase present in M3 than in M1 and M2, proving that the $\alpha$-phase increases as the ZnO amount decreases and the PVDF amount increases.

The fraction of $\beta$-phase ($F_\beta$) can be calculated using Equation (1) derived from the Beer-Lambert Law [33]:

$$F_\beta = \frac{A_\beta}{\left(\left[1.3A_\alpha\right] + A_\beta\right)} \tag{1}$$

where $A_\alpha$ is the absorbance at 766 $cm^{-1}$ and $A_\beta$ is the absorbance at 840 $cm^{-1}$ [33]. According to Equation (1), the $\beta$-phase content calculated in M1 is 76.47%, in M2 is 72.17%, and in M3 is 51.29%.

The analysis of FTIR absorption spectra indicates that the fraction of the piezoelectric $\beta$-phase in the sample fabricated using the ratio in M1 or M2 is significantly higher than the sample fabricated using the ratio in M3. M1 has the highest fraction of the $\beta$-phase. Thus, it can be concluded that the percent of $\beta$-phase increases as the percent of ZnO increases.

### 4.6. Tensile Test Findings

Both M2 and M3 had the same dimensions (same length, width, and thickness). The methodology described in [34] was followed to calculate stiffness. Data before the yield point (**Figure 14**) demonstrated the stiffness of M2 and M3 as 4.135 N/mm and 3.311 N/mm respectively, indicating that M2 is more brittle than M3. The maximum and yield loads of M2 are higher than M3 - M2 withstood a maximum load of 2.417 N while M3 only withstood 2.348 N before breakage. Thus, the ultimate tensile strength of M2 was greater than M3. The elongation percentage of both membranes was calculated using the formula described in [35], as 7.1% for M2 and 8.6% for M3, demonstrating the higher flexibility of M3.

Based on these calculations and analyses, increasing the amount of ZnO within the membranes increased strength and brittleness but decreased flexibility.

### 4.7. Prototype and Proof of Concept

A prototype system was designed to mimic the natural biological response to bending, tapping, and pushing [36]. The schematic of this prototype is shown

(Figure 15). The membrane is sandwiched between two electrodes and encased in an insulating material. Two leads are attached to the electrodes. When subjected to external stimuli, the prototype should convert mechanical energy to an electrical signal due to the piezoelectric effect. A voltmeter connected to the two leads of the prototype reads this signal.

In order to make the prototype, a 2 in × 2 in section of the membrane was prepared. Flexible copper tape with one side coated with conductive glue was used as electrodes on both the top and bottom surfaces of the membrane. Silver conductive ink, which dries at room temperature, was used to attach copper wires to the electrodes, and in turn, the copper wires were connected to a voltmeter (Figure 16). Tapping, pushing on, and bending the prototype resulted in a non-zero voltmeter reading (Figure 17).

### 4.8. Limitations and Future Research

Since the researcher is a high school student, there was limited access to specialized equipment (electrospinner, SEM, XRD, FTIR, stress-strain testing equipment). Consequently, there were fewer samples used in testing. Further research

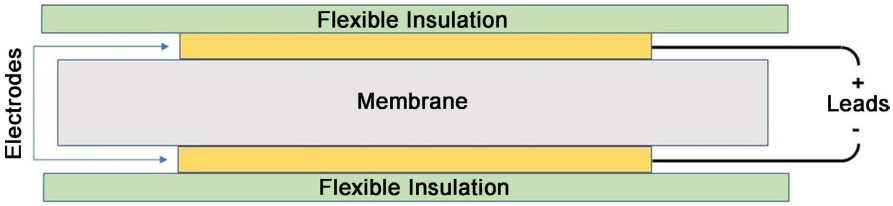


Figure 15. Schematic of a nanogenerator.

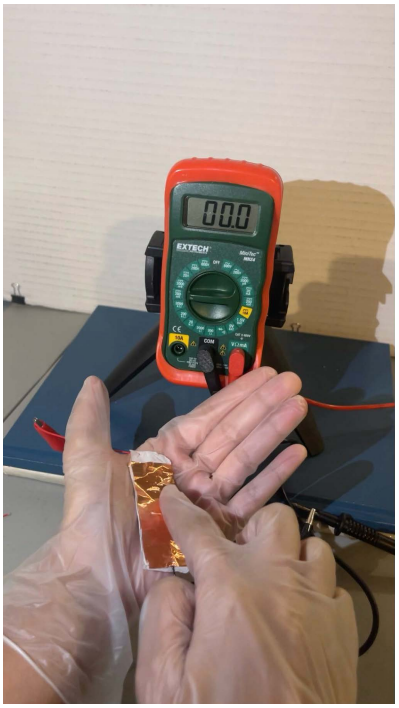


Figure 16. Initial voltmeter reading of zero.


**Figure 17.** Non-zero voltmeter reading as prototype is subjected to mechanical stresses.

can be performed with a larger sample size and additional ratios to establish an optimum range of ratios of PVDF to ZnO. Testing antibacterial activity and surface wettability would also provide valuable information. Further investigation could reveal ways to improve the synthetic pathway and evaluate yield rates for commercial applications.

## 5. Conclusion

Within the stated limitations, this study supports the hypothesis that changing the amount of ZnO changes the piezoelectric potential of PVDF, and successfully establishes that an electrospun membrane with a 1:1 ratio of PVDF to ZnO by weight is optimal to create a flexible, biocompatible, and piezoelectric nanocomposite. The manifestation of these properties proves that this material has a high potential to be integrated into treatments for sensory receptor damage. The novelty of the experiment is that analysis of different ratios for this purpose, with DMSO as a solvent, has never been conducted before. Furthermore, this process does not use hazardous compounds, and the resultant membrane is piezoelectric, biocompatible, and flexible.

## Acknowledgements

This study would not have been feasible without the assistance of several individuals who extended their support to me. First and foremost, I would like to thank my TAG teacher, Ms. Santhi Prabahar, for her day-to-day guidance, helpful suggestions, and encouragement. I would also like to thank Dr. Suresh Sitaraman and Dr. Rui Chen (Georgia Tech) for supporting my research by provid-

ing equipment access and support for stress-strain testing. Additionally, I am grateful for the technical assistance and help with SEM imaging provided by Dr. Pankaj Rohilla (Georgia Tech). Finally, I would also like to thank the COMSAT lab for electrospinning membranes per my specifications, and for providing raw XRD and FTIR data in CSV files.

## Conflicts of Interest

The author declares no conflicts of interest regarding the publication of this paper.

## References

[1] World Health Organization (2018) Burns. https://www.who.int/news-room/fact-sheets/detail/burns

[2] McDermott, K.W., Weiss, A.J. and Elixhauser, A. (2017) Burn-Related Hospital Inpatient Stays and Emergency Department Visits, 2013. Agency for Healthcare Research and Quality (US), Rockville. https://europepmc.org/article/nbk/nbk409513

[3] Dixit, S., Baganizi, D.R., Sahu, R., Dosunmu, E., Chaudhari, A., Vig, K., Pillai, S.R., Singh, S.R. and Dennis, V.A. (2017) Immunological Challenges Associated with Artificial Skin Grafts: Available Solutions and Stem Cells in Future Design of Synthetic Skin. *Journal of Biological Engineering*, **11**, Article No. 49. https://doi.org/10.1186/s13036-017-0089-9

[4] UVA Health (2022) Skin Graft. https://uvahealth.com/services/plastic-surgery/skin-graft

[5] World Health Organization (2021) Deafness and Hearing Loss. https://www.who.int/news-room/fact-sheets/detail/deafness-and-hearing-loss

[6] Kampsen Hearing (2020) What Are the Pros and Cons of Cochlear Implants. https://kampsenhearing.com/what-are-the-pros-and-cons-of-cochlear-implants

[7] İlik, B., Koyuncuoğlu, A., Şardan-Sukas, Ö. and Külah, H. (2018) Thin Film Piezoelectric Acoustic Transducer for Fully Implantable Cochlear Implants. *Sensors and Actuators A*: *Physical*, **280**, 38-46. https://doi.org/10.1016/j.sna.2018.07.020

[8] Lin, W., Wang, B., Peng, G., Shan, Y., Hu, H. and Yang, Z. (2021) Skin-Inspired Piezoelectric Tactile Sensor Array with Crosstalk-Free Row + Column Electrodes for Spatiotemporally Distinguishing Diverse Stimuli. *Advanced. Science*, **8**, Article ID: 2002817. https://doi.org/10.1002/advs.202002817

[9] Kim, D.W., Kim, H., Hwang, G.-T., Cho, S.B., Jeon, S.H., Kim, H.W., Jeong, C.K., Chun, S. and Pang, C. (2022) Conformably Skin-Adherent Piezoelectric Patch with Bioinspired Hierarchically Arrayed Microsuckers Enables Physical Energy Amplification. *ACS Energy Letters*, **7**, 1820-1827. https://doi.org/10.1021/acsenergylett.2c00259

[10] Stöver, T. and Lenarz, T. (2011) Biomaterials in Cochlear Implants. *GMS Current Topics in Otorhinolaryngology, Head and Neck Surgery*, **8**, Doc10.

[11] Sekhar, B.C., Dhanalakshmi, B., Rao, B.S., Ramesh, S., Prasad, K.V., Rao, P.S.V.S. and Rao, B.P. (2021) Piezoelectricity and Its Applications. In: Sahu, D.R., Ed., *Multifunctional Ferroelectric Materials*, IntechOpen, London, 71-88. https://www.intechopen.com/chapters/77225

[12] Zaszczynska, A., Sajkiewicz, P. and Gradys, A. (2020) Piezoelectric Scaffolds as Smart Materials for Neural Tissue Engineering. *Polymers*, **12**, Article 161.

https://doi.org/10.3390/polym12010161

[13] Ruan, L., Yao, X., Chang, Y., Zhou, L., Qin, G. and Zhang, X. (2018) Properties and Applications of the $\beta$ Phase Poly(vinylidene fluoride). *Polymers*, **10**, Article 228. https://doi.org/10.3390/polym10030228

[14] Taleb, S., Badillo-Avila, M.A. and Acuautla, M. (2021) Enhanced Performance of Flexible Piezoelectric PVDF Sensors by Ultrasonic Spray Coating Method. 2021 *IEEE International Symposium on Applications of Ferroelectrics* (*ISAF*), Sydney, 16-21 May 2021, 1-4. https://doi.org/10.1109/ISAF51943.2021.9477342

[15] Sigma-Aldrich (2021) Safety Data Sheet Revision Date 01/21/2021 Version 6. https://www.sigmaaldrich.com/US/en/sds/ALDRICH/182702

[16] Mahalakshmi, S., Hema, N. and Vijaya, P.P. (2020) *In Vitro* Biocompatibility and Antimicrobial Activities of Zinc Oxide Nanoparticles (ZnO NPs) Prepared by Chemical and Green Synthetic Route—A Comparative Study. *BioNanoScience*, **10**, 112-121. https://doi.org/10.1007/s12668-019-00698-w

[17] Srikanth, K.S., Wazeer, A., Mathiyalagan, P., Vidya, S., Rajput, K. and Kushwaha, H.S. (2021) 25—Piezoelectric Properties of Zno. In: Awasthi, K., Ed., *Nanostructured Zinc Oxide*: *Synthesis*, *Properties and Applications*, Elsevier, Amsterdam, 717-736. https://doi.org/10.1016/B978-0-12-818900-9.00024-3

[18] Mendes, C., Dilarri, G., Forsan, C.N., De Moraes Ruy Sapata, V., Lopes, P.S., De Moraes, P.B., Montagnolli, R.N., Ferreira, H.B. and Bidoia, E.D. (2022) Antibacterial Action and Target Mechanisms of Zinc Oxide Nanoparticles against Bacterial Pathogens. *Scientific Reports*, **12**, Article No. 2658. https://doi.org/10.1038/s41598-022-06657-y

[19] Wille, A., Mishra, Y.K., Gedamu, D., Paulowicz, I., Jin, X. and Adelung, R. (2011) Zinc Oxide Micro- and Nanostructures as Multifunctional Materials. SPIE—The International Society of Optics and Photonics Search. https://doi.org/10.1117/2.1201111.003944 https://spie.org/news/3944-zinc-oxide-micro--and-nanostructures-as-multifunctional-materials?SSO=1

[20] Bhadwal, N., Mrad, R.B. and Behdinan, K. (2023) Review of Zinc Oxide Piezoelectric Nanogenerators: Piezoelectric Properties, Composite Structures and Power Output. *Sensors*, **23**, Article 3859. https://doi.org/10.3390/s23083859

[21] Meringolo, C., Mastropietro, T.F., Poerio, T., Fontananova, E., De Filpo, G., Curcio, E. and Di Profio, G. (2018) Tailoring PVDF Membranes Surface Topography and Hydrophobicity by a Sustainable Two-Steps Phase Separation Process. *ACS Sustainable Chemistry & Engineering*, **6**, 10069-10077. https://doi.org/10.1021/acssuschemeng.8b01407

[22] National Institute for Occupational Safety and Health (2014) Preventing Adverse Health Effects from Exposure to: Dimethylformamide (DMF) https://www.cdc.gov/niosh/docs/90-105/default.html

[23] Marshall, J.E., Zhenova, A., Roberts, S., Petchey, T., Zhu, P., Dancer, C.E.J., McElroy, C.R., Kendrick, E. and Goodship, V. (2021) On the Solubility and Stability of Polyvinylidene Fluoride. *Polymers*, **13**, Article 1354. https://doi.org/10.3390/polym13091354

[24] Gaylord Chemical (2022) Dimethyl Sulfoxide (DMSO) Health and Safety. https://www.gaylordchemical.com/environmental-health-safety/dmso-health-safety

[25] AZoNano.com (2022) An Introduction to Electrospinning and Nanofibers. https://www.azonano.com/article.aspx?ArticleID=4377

[26] Bioinicia (2018) Electrospinning Device for Medical Applications.

https://bioinicia.com/electrospinning-device-medical-applications

[27] Hasnidawani, J.N., Azlina, H.N., Norita, H., Bonnia, N.N., Ratim, S. and Ali, E.S. (2016) Synthesis of ZnO Nanostructures Using Sol-Gel Method. *Procedia Chemistry*, **19**, 211-216. https://doi.org/10.1016/j.proche.2016.03.095

[28] Kalimuldina, G., Turdakyn, N., Abay, I., Medeubayev, A., Nurpeissova, A., Adair, D. and Bakenov, Z. (2020) A Review of Piezoelectric PVDF Film by Electrospinning and Its Applications. *Sensors*, **20**, Article 5214. https://doi.org/10.3390/s20185214

[29] Yin, Z., Tian, B., Zhu, Q. and Duan, C. (2019) Characterization and Application of PVDF and Its Copolymer Films Prepared by Spin-Coating and Langmuir-Blodgett Method. *Polymers*, **11**, Article 2033. https://doi.org/10.3390/polym11122033

[30] Cai, X., Lei, T., Sun, D. and Linde, L. (2017) A Critical Analysis of the $\alpha$, $\beta$ and $\gamma$ Phases in Poly(Vinylidene Fluoride) Using FTIR. *RSC Advances*, **7**, 15382-15389. https://doi.org/10.1039/C7RA01267E

[31] Upadhyay, P., Jain, V., Sharma, S., Shrivastav, A.B. and Sharma, R. (2020) Green and Chemically Synthesized ZnO Nanoparticles: A Comparative Study. *IOP Conference Series*, **798**, Article ID: 012025. https://doi.org/10.1088/1757-899X/798/1/012025

[32] Cowger, W., Steinmetz, Z., Gray, A., Munno, K., Lynch, J., Hapich, H., Primpke, S., De Frond, H., Rochman, C. and Herodotou, O. (2021) Microplastic Spectral Classification Needs an Open Source Community: Open Specy to the Rescue! *Analytical Chemistry*, **93**, 7543-7548. https://doi.org/10.1021/acs.analchem.1c00123

[33] Kumarasinghe, H.U., Bandara, L.R.A.K., Bandara, T.M.W.J., Senadeera, G.K.R. and Thotawatthage, C.A. (2021) Fabrication of $\beta$-Phase Poly(vinylidene fluoride) Piezoelectric Film by Electrospinning for Nanogenerator Preparations. *Ceylon Journal of Science*, **50**, 357-363. https://doi.org/10.4038/cjs.v50i5.7925

[34] Goodyear, S. and Aspden, R. (2012) Mechanical Properties of Bone *ex Vivo*. In: Helfrich, M. and Ralston, S., Eds., *Bone Research Protocols*, Vol. 816, Humana Press, Totowa, NJ, 555-571. https://doi.org/10.1007/978-1-61779-415-5_35

[35] TWI Global (2015). https://www.twi-global.com/technical-knowledge/job-knowledge/mechanical-testing-tensile-testing-part-1-069

[36] Hu, J.Y., Gu, Y.Y., Zhang, H.L., *et al.* (2018) Effect of Electrode Material on Piezoelectric Output of PVDF Sensor with Electrospun Nanofiber Web. *Advanced Materials Letters*, **9**, 363-368. https://doi.org/10.5185/amlett.2018.1958